A GPS Velocity Sensor: How Accurate Can It Be? – A First Look

Luis Serrano, Donghyun Kim and Richard B. Langley
Department of Geodesy and Geomatics Engineering
University of New Brunswick, Canada

Kenji Itani
Furuno Electric Co., Ltd., Nishinomiya, Japan

Mami Ueno
CNRS I3S Laboratory, Sophia Antipolis, France

BIOGRAPHIES

Luis Serrano obtained his Diploma in geographic engineering from the Faculty of Sciences of the University of Lisbon. During the past 4 years he has been working in geodetic engineering. Currently he is an M.Sc.Eng. student in the Department of Geodesy and Geomatics Engineering at the University of New Brunswick, where he carries out research in precise navigation.

Donghyun Kim is a research associate in the Department of Geodesy and Geomatics Engineering at the University of New Brunswick, where he has developed the UNB RTK software for a gantry crane auto-steering system. He has a B.Sc., M.Sc. and Ph.D. in geomatics from Seoul National University. He has been involved in GPS research since 1991. Currently, Dr. Kim carries out research related to ultrahigh-performance RTK positioning at up to a 50 Hz data rate, with application to real-time deformation monitoring, Internet-based moving platform tracking, and machine control.

Richard B. Langley is a professor in the Department of Geodesy and Geomatics Engineering at the University of New Brunswick, where he has been teaching and conducting research since 1981. He has a B.Sc. in applied physics from the University of Waterloo and a Ph.D. in experimental space science from York University, Toronto. Professor Langley has been active in the development of GPS error models since the early 1980s and is a contributing editor and columnist for GPS World magazine.

Kenji Itani is a chief engineer in the Research Division of Furuno Electric Co., Ltd., Nishinomiya, Japan. He received his B.S.E.E. and M.S.E.E. from Kobe University in 1971 and 1973, respectively. He has been involved in the development of GPS receivers since 1991 as a software engineer. He is currently developing carrier-phase applications with low-cost GPS receivers.

Mami Ueno obtained her Ph.D. in geomatic sciences from Laval University, Canada and her B.Sc. and M.Sc. in marine systems engineering from Tokyo University of Mercantile Marine, Japan. She has worked on the development of GPS data processing algorithms and software. Dr. Ueno is currently working on underwater robot navigation as a research fellow at CNRS I3S signal processing laboratory, Sophia Antipolis, France.

ABSTRACT

To obtain accurate velocity information, traditional optical velocity sensors and RTK-GPS positioning are common but expensive solutions. However, velocity information can be obtained from the time-differential method using a stand-alone single-frequency receiver without resolving carrier phase ambiguities. In dynamic vehicle testing, such a GPS sensor is attractive because it enables a single person to conduct performance tests quickly and easily.

We have investigated the feasibility of a low-cost GPS velocity sensor for applications such as vehicle testing. We developed post-processing software which uses the first order central difference approximation of the carrier-phase rate. The advantage of this approximation is simplicity, which facilitates implementation of algorithms into the receiver. In this paper, we mainly focus on the scientific aspects of the GPS velocity determination. We investigated the potential accuracy which can be achieved with low-cost receivers, and evaluated the error budget present in the estimation. The algorithms consider specifically data smoothing, multipath, and modeling of

ionospheric effects as well as efficient handling of cycle slips and other data anomalies.

We conducted field tests to evaluate the performance of Furuno's low-cost single-frequency GPS receiver for a static and a kinematic case. In static mode, the user velocity has been estimated to be better than 1 cm/s (2-sigma) in a high-multipath environment. In kinematic mode, we observed the increase of receiver dynamics in the residuals. However, we did not experience any long signal interruption even under high multipath.

Using the Doppler measurements (either the receiver-generated Doppler or the carrier-phase derived Doppler) observed from a moving platform, it is easy to determine the velocity of the platform as long as the satellite velocity is precisely known.

From our early results, we confirmed that the satellite velocity predicted by using the broadcast ephemeris in the navigation message is comparable to the velocity of NGA (National Geospatial Intelligence agency) SP3 precise ephemeris. The errors in the position of a moving vehicle cause an error in the calculation of radial velocity. For stand-alone velocity determination, in order to achieve a solution at the mm/s level, satellite positions have to be known better than 10 m.

This paper describes the algorithm developed at UNB, results and analysis of the field tests and future work to be done.

INTRODUCTION

Previous studies on GPS velocity determination show that it is possible to achieve accuracies of a few millimetres per second depending on receiver quality, whether in static or kinematic mode, stand-alone or relative mode, and the particular dynamics situation [Van Graas and Soloviev, 2003; Ryan et al., 1997]. The velocity of the receiver mounted on a moving platform can be determined by using the carrier-phase derived Doppler measurements or the receiver generated Doppler measurements.

As is well known, a GPS receiver conducts a search over the space of the Doppler-frequency shift and the code-phase shift at the signal acquisition stage. The receiver-generated Doppler measurements correspond to the Doppler shift estimated by the ambiguity function used in the search. The accuracy of the Doppler-shift estimates depends on the size of Doppler bin used in the search [Misra and Enge, 2001]. The receiver-generated Doppler is usually noisier than the carrier-phase-derived Doppler.

A receiver-generated Doppler measurement is a measure of instantaneous velocity, whereas the carrier-phase-derived Doppler is a measure of mean velocity between observation epochs. The Doppler measurement is noisier than carrier-phase-derived Doppler because the receiver-generated Doppler is measured over a very small time interval. As carrier-phase-derived Doppler is computed over a longer time span than Doppler, the random noise is averaged and lowered. Therefore, very smooth velocity is obtained by carrier-phase-derived Doppler observation if there is no undetected cycle slips.

The carrier-phase-derived Doppler can be obtained by either differencing carrier phase observations in the time domain, normalizing them with the time interval of the differenced observations or by fitting a curve using polynomials of various orders with successive phase measurements (delta-ranges). In our investigation, we were interested in estimating the velocity for relatively low-velocity and low-dynamics environments. We used the first order central difference approximation of the carrier-phase rate to generate the Doppler observations. As was demonstrated by Szarmes et al. [1997], this approach is easy to implement and also provides the most appropriate velocity estimates in low dynamics environments.

Velocity determination algorithms described in the following section can be implemented on different platforms. Some applications using such algorithms are described in Itani et al. [2000] and Okamura et al. [2003]. The latter describes the tests performed on a racing circuit using the time-differential carrier-phase observations from a stand-alone GPS receiver. The simple algorithms using a low-cost receiver such as the GN-77, Furuno's 12-channel GPS receiver were reported to achieve an accuracy of 5 mm/s (1 sigma).

We can imagine easily other areas of applications using such receivers. For example, in agricultural applications, it is important to control the quantity of pesticides or fertilisers applied on farms. An accurate velocity determination contributes to spreading chemicals evenly, sowing seeds or planting seedlings with even spacing on a straight line, which facilitates the management of the farm fields.

Figure 1: Experiment on a farm vehicle

Figure 1 shows an experiment of running a tractor straight ahead automatically using a GPS velocity sensor.

Figure 2: Antenna installed on the vehicle used for the farm experiment

Figure 2 shows the antenna installed on the tractor used in the experiments [Ueno et al; 2003].

GPS VELOCITY DETERMINATION

The following discusses our approach for velocity determination using GPS. Although our approach provides velocity and point positioning solutions at the same time, we focus on only the velocity part which is described in 5 steps as shown in Figure 3. We developed post-processing software which uses the first order central difference approximation of the carrier-phase rate expressed in Equation (1). The advantage of this approximation is simplicity, which facilitates eventual implementation of algorithms into a receiver.

$$\dot{\Phi}_k^j \approx \frac{\Phi_{k+\Delta t}^j - \Phi_{k-\Delta t}^j}{2 \cdot \Delta t}, \qquad (1)$$

where Φ is the carrier-phase observation; superscript j represents the satellite; subscripts k and Δt are the observation epoch and time interval of the observation, respectively.

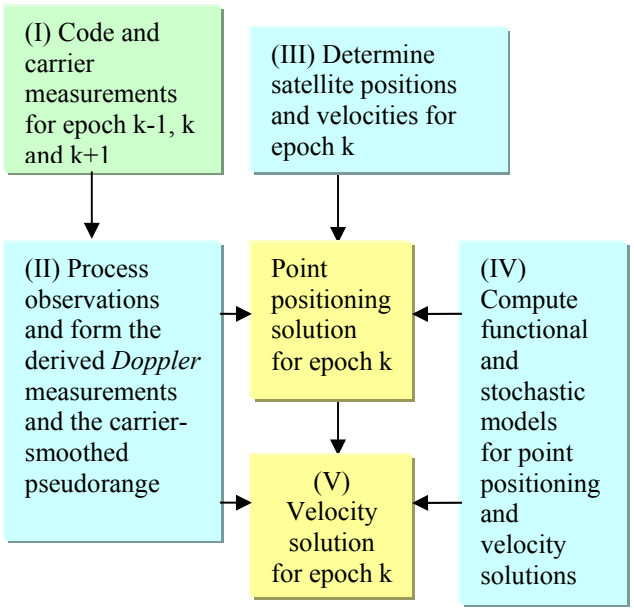

Figure 3: GPS velocity determination procedures

Step I:
The first step of our approach is to compute an approximate user position. For the velocity determination, we need approximate user positions not only at the present epoch, but also at the previous and next epochs as input parameters. We use both code and phase measurements to estimate user positions. The errors in the position of a moving vehicle cause an error in the calculation of the radial component of the platform-satellite velocity vector. The magnitude of error is about 1 cm/s for a position error of 100 m in relative velocity determination. The precise determination of position is important to the precise determination of velocity. At least, positioning accuracy of DGPS, *i.e.*, 10 m, is required for the errors caused by the wrong coordinates to be negligible [Itani et al. 2000]. For stand-alone velocity determination, in our investigation, we tested and confirmed that an error of 100 m in the position could result in 4 cm/s of bias errors in velocity in particular in the vertical component. An error of 10m in the position could provide the velocity estimation without deviation. In this case, errors were absorbed in the least-squares solution and we obtained a noisier solution with an error of few mm/s.

Step II:
In the first step, we process the raw measurements (both code and phase). In this step, we form carrier-phase-derived Doppler and carrier-smoothed pseudoranges. Equation (2) shows the observation equation for the velocity determination.

$$\dot{\Phi}_k^j = \dot{\rho}_k^j + (\dot{B}_k - \dot{b}_k^j) + \dot{I}_k^j + \dot{T}_k^j + e_k \qquad (2)$$

Where $\dot{\rho}$ stands for the geometric range rate between the receiver and satellite; $\dot{B}$ for the receiver clock drift; $\dot{b}$ for the satellite clock drift; $\dot{I}$ for the ionospheric delay rate; $\dot{T}$ for the tropospheric delay rate and e for the receiver system noise.

We model out some of the errors in the observations. They are the errors in satellite clock, propagation effects in the ionosphere and troposphere, and receiver system noise, which can be summarised as in Equation (3):

$$\varepsilon_k^j = -\dot{b}_k^j + \dot{I}_k^j + \dot{T}_k^j + e_k \qquad (3)$$

The effects of satellite clock bias and drift were modeled out using the coefficients in the navigation message [ICD-GPS-200, 1999]. The relativistic effect and group delay differential are also accounted for using appropriate algorithms with values given in the navigation message. To reduce the effect of the tropospheric delay in the measurements, we use the UNB3 tropospheric prediction model [Collins and Langley, 1997], which is based on the zenith delay algorithms of Saastamoinen [1973], the mapping functions of Niell [1996], and a table of sea-level atmospheric values derived from the U.S. 1966 Standard Atmosphere Supplements, and lapse rates to scale the sea-level values to the receiver height. For reducing the effects of ionospheric delay, we use the standard (Klobuchar) model using the parameter values in the navigation message. Since we use the time-differenced measurements over a short time interval (that is, less than or equal to 2 seconds) for velocity determination, the residual effects of the tropospheric and ionospheric delays, if any, are normally negligible.

After modeling accordingly the measurements, the observation equation for velocity determination is now given by the following:

$$\dot{\Phi}_k^j = \mathbf{h}_k^j.(\mathbf{v}_k^j - \mathbf{V}_k) + \dot{B}_k + \varepsilon_k^j \qquad (4)$$

where **v** stands for the satellite velocity vector; **V** for the receiver velocity vector; and **h** represents the directional cosine vector between the receiver and satellite and is given by:

$$\mathbf{h}_k^{jT} = \frac{\left(\mathbf{X}_k^j - \mathbf{u}_k\right)}{\left|\mathbf{X}_k^j - \mathbf{u}_k\right|}, \qquad (5)$$

where **X** and **u** represent the satellite and receiver positions, respectively.

Step III:
In Step 3, we get estimates of satellite positions and velocities for epoch k. In order to get these estimates as additional inputs for the velocity determination, we use the satellite ephemeris in the navigation message.

Step IV:
In Step 4, we compute functional and stochastic models for point positioning and velocity solutions. From Equation (4), we obtain the functional model for velocity determination, which is given by:

$$\dot{\mathbf{\Phi}}'_k = \mathbf{G}_k \cdot \mathbf{x}_k + \boldsymbol{\varepsilon}_k \qquad (6)$$

and

$$\begin{aligned} \dot{\mathbf{\Phi}}'_k &= \dot{\mathbf{\Phi}}_k - \mathbf{H}_k \cdot \mathbf{v}_k \\ \mathbf{G}_k &= \begin{bmatrix} \mathbf{H}_k & \mathbf{1} \end{bmatrix} \\ \mathbf{x}_k &= \begin{bmatrix} -\mathbf{V}_k^T & \dot{B}_k \end{bmatrix}^T, \end{aligned} \qquad (7)$$

where **H** is the design matrix including all directional cosine vectors between the receiver and satellite; and **1** is a column vector having 1s as its elements.

The formulation of the stochastic model **Q** for velocity determination is based on the assumption that the relationship between satellite elevation angle and system noise can be quite well modeled by an exponential function [Jin, 1996]. Since most of the biases and errors in the measurements will be cancelled in the first order central difference approximation of the carrier-phase rate, such an assumption can be easily justified.

Assuming no temporal correlation in the carrier phase observations and no correlation among the receiver channels, we will have:

$$\mathbf{Q}_{\dot{\mathbf{\Phi}}'_k} = \begin{bmatrix} \sigma^2_{\dot{\Phi}^1_k} & & & \\ & \sigma^2_{\dot{\Phi}^2_k} & & \\ & & \ddots & \\ & & & \sigma^2_{\dot{\Phi}^n_k} \end{bmatrix}, \qquad (8)$$

where

$$\sigma^2_{\dot{\Phi}^j_k} = \frac{1}{4 \cdot \Delta t^2}\left(\sigma^2_{\Phi^j_{k+\Delta t}} + \sigma^2_{\Phi^j_{k-\Delta t}}\right). \qquad (9)$$

Furthermore, the variance of the first order central difference approximation of the carrier-phase rate will be used to fit the exponential function as:

$$\sigma^2_{\Phi^j_k} = a_0 + a_1 \exp\left(\frac{a_2}{ELEV^j_k}\right), \qquad (10)$$

where *ELEV* represents the elevation angle of the satellite. In order to model the system noise, we need to estimate correctly the coefficients a_0, a_1 and a_2 in Equation (10). The first two coefficients are expressed in metres and the third one is in degrees. We estimated these coefficients by means of the least-squares estimation, using our first test data for the static case (Fig. 4) prior to our successive tests (see below).

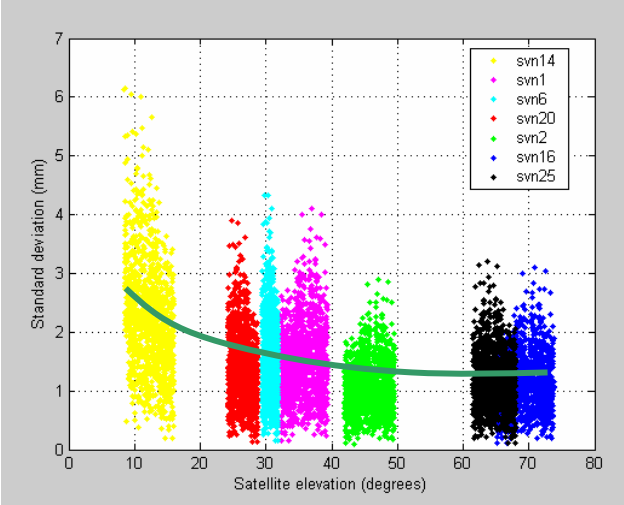

Figure 4: Exponential function that models the relation between the satellites elevation and the observations precision

As we can see from Fig. 4, the assumption between the satellite elevation angle and system noise being modeled by an exponential function, for the static case, works fairly well.

Step V:
In Step 5, we now obtain the velocity solution for epoch k. After the formulation of the functional and stochastic models, it is easy to implement the main processor, the least-squares sequential estimator. As we are still at the development phase, the velocities are determined separately from the position estimates. Later on, the position and velocity components will be combined in the same state vector for further navigation solutions.

TEST RESULTS

In order to verify the performance of our approach, we conducted a series of tests. The first test was performed in static mode on the roof of the Gillin Hall engineering building at UNB. As depicted in Figure 5, the test was carried out in a multipath-rich environment. Test data were recorded at a 1 Hz data rate for about 20 minutes. Furuno's software MONI77.EXE, which has a simple and easy-to-use interface, was used for recording the data.

Figure 5: Static test in a multipath-rich environment.

Figure 6 shows the results of velocity determination. We summarize the statistics of the results in Table 1, giving the mean, standard deviation (std.) and root-mean-square (r.m.s.) of the velocity components as well as the speed. Since this test was carried out in static mode, the velocity estimates were compared with the expected zero velocity values as the truth. We see some of the errors (incorrectly modelled or a part of which is not modelled) were absorbed in the least-squares solution and caused some bias in velocity solutions, particularly in the vertical component. However, we can still confirm that velocity determination using the first order central difference approximation of the carrier-phase rate performed quite well in the static mode.

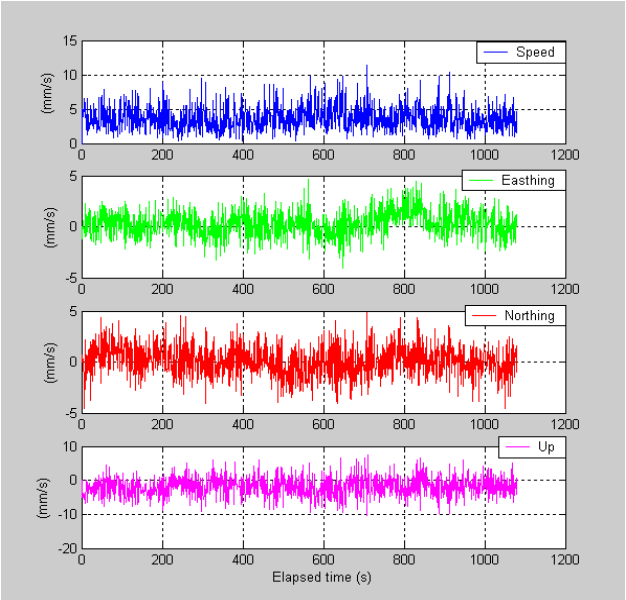

Figure 6: Velocity estimates from the static-mode test. Top panel shows the speed estimates and the bottom three panels illustrate Northing, Easting and Up components of the velocity estimates

	Northing	*Easting*	*Up*	*Speed*
mean	0.09	0.10	-2.01	3.67
std.	1.2	1.2	3.0	1.8
rms	1.3	1.3	3.6	4.0

Table 1: Statistics of static-mode test under multipath-rich conditions (unit: mm/s)

Another unknown parameter in the functional model for velocity determination is the receiver clock drift. Figure 7 shows the receiver clock bias and drift estimates. The receiver clock biases were estimated by the carrier-phase-smoothed pseudoranges using the Hatch-type filter [Hatch, 1982].

The receiver clock drifts $\dot{B}$, were independently estimated by Eq. (6).

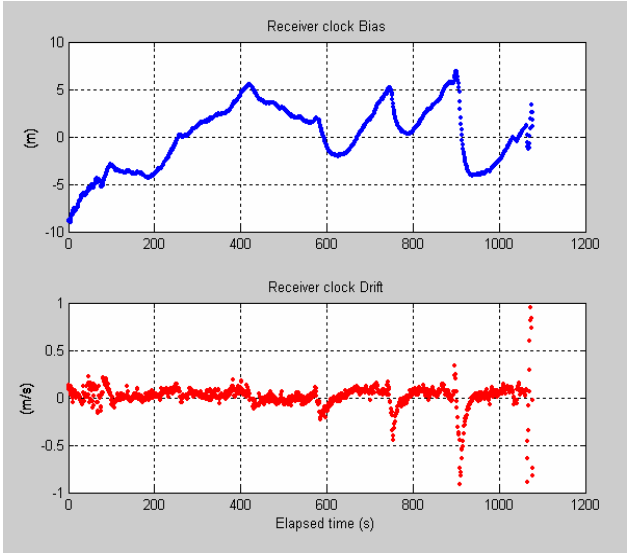

Figure 7: Receiver clock bias (top) and drift (bottom) estimates

Factors which can affect (actually, hide in) the estimates of the receiver clock drift may include the residuals of the satellite velocity prediction, the higher-order effects of the user (i.e., receiver) dynamics and errors such as residual atmospheric (ionospheric and tropospheric) delay, multipath and receiver system noise.

The residuals of the satellite velocity prediction may not affect significantly the estimates of the receiver clock drift. In order to verify this assumption, we compared them with those predicted from broadcast ephemerides using the NGA SP3 satellite velocities as a truth reference. Table 2 summarises the results of comparison expressed in ECEF coordinates. From the values for two consecutive epochs (30 minute arc) in the difference between the velocities obtained from the broadcast and NGA SP3 velocities, we could consider the satellite velocity accuracy to be 1-2 mm/s. We could further assume that satellite velocity errors propagate into the user velocity with the same magnitude.

Vx (mm/s)	*Vy (mm/s)*	*Vz (mm/s)*
1.325	1.123	1.209

Table 2: Root-mean-square differences of broadcast satellite velocities and SP3 satellite velocities

For this test, the higher-order effects of receiver dynamics are negligible as the test was carried out in the static mode. The higher-order effects of the atmospheric delay in the first order central difference approximation of the carrier- phase rate, if any, are insignificant in our test as the test was conducted at a 1 Hz data rate. Furthermore,

no severe solar storm which can cause ionospheric scintillation (contributing to the higher-order effects of the ionospheric delay) took place during the test.

As is illustrated in the bottom panel of Figure 7, the estimates of the receiver clock drift show to some degree cyclic behaviour. The time constant of this behaviour is about 180 seconds. The cause of this behaviour may come from either the receiver clock itself or perhaps multipath. We could say, however, this is not particularly related to the rising or setting of satellites. In this session, we had 7 satellites, of which 6 satellites had an elevation angle more than 20 degrees and only one less than 10 degrees as shown in Figure 4.

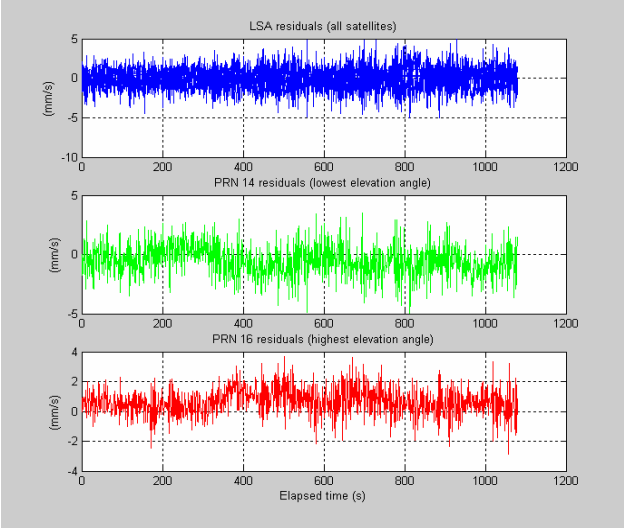

Figure 8: Residuals of the least-squares estimation with the residuals for satellites PRN 14 with the lowest elevation angle and 16 with the highest elevation angle, separately shown

To see whether or not higher-order effects of multipath might be influencing the estimates of the receiver clock drift, especially the cyclic behaviour of the estimates, we analyzed the residuals of the least-squares estimation as illustrated in Figure 8, which show some cyclic behavior. When we compare the results of receiver clock bias and clock drift in Figure 7, we see some correspondence in the epochs where the large errors are present.

From this fact, we could say that there were large errors from different origins such as multipath, model errors and receiver internal errors. It could be said that some of the errors were absorbed in the solutions and some was left as residuals. When the systematic errors such as bias or drift are present in the residuals, the integrated residuals reveal this fact. The integrated residuals have cumulative effects as time elapses with systematic errors.

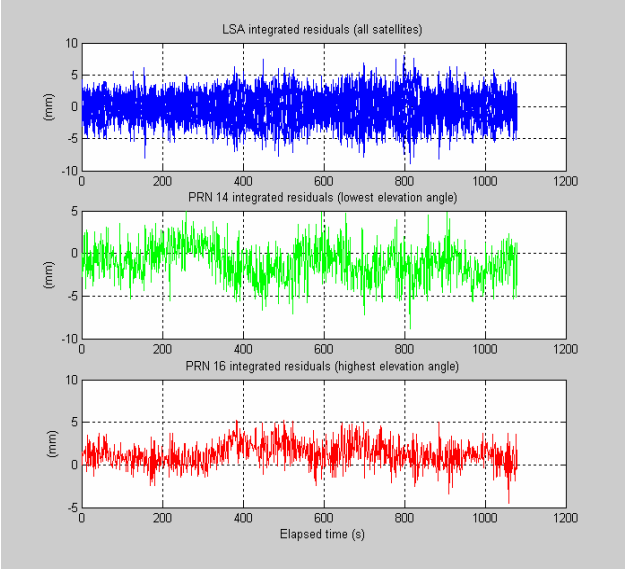

Figure 9: Integrated residuals of the least-squares estimation

Figure 9 show a typical example of the integrated residuals of the satellites at low and high elevation angles, just like in Figure 8. Figure 9 did not reveal the cumulative effect. No significant multipath (or multipath-like signature) is found in Figure 9. From this fact, we could conclude that the cyclic behavior might be related to the receiver clock drift, when these large errors were of internal origin.

Kinematic Test

The second test was performed in kinematic mode. We put the antenna on the top of a car (Figure 10) and drove from the university to the downtown of Fredericton and then onto a highway. For analysis, we processed a small part (about 6 minutes) of the data recorded during this test. This 6-minute data set represents the time period when the car stopped for a few minutes in the downtown and then moved onto the highway. The car reached the speed limit (110 km/h or around 30 m/s) very quickly after entering the highway and maintained the speed for a few minutes.

Figure 10: System setup for kinematic test

During the kinematic test, Furuno's velocity determination software informed us of the speed of the car in real-time. This enabled us to confirm the approximate consistency of the speeds determined by the vehicle's speedometer and the software.

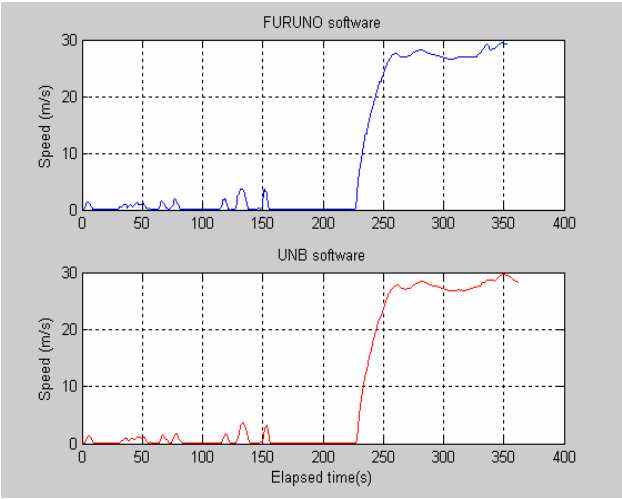

Figure 11: Comparison of the speeds determined in the kinematic mode using the Furuno and UNB software

By logging the raw pseudorange and carrier-phase data during the test and post-processing them later on, we could also compare the results of the Furuno software with those of the UNB velocity-determination software. Figure 11 shows an example of the comparison of velocity determination using both Furuno's and UNB's software. The two results agreed for most of the time except during the period (340-350 seconds) where the receiver tracked only 4 satellites. In that period, the two solutions show some difference, which is probably because modeling some errors with fewer degrees of freedom has some influence on the velocity solutions.

Figure 12 shows the velocity estimates from the UNB software.

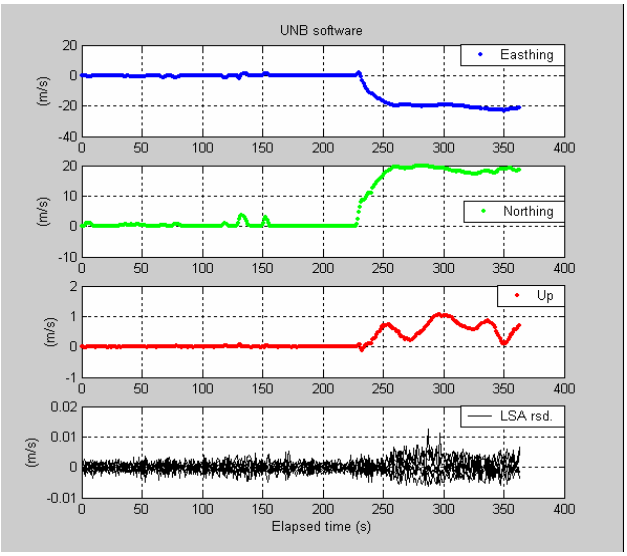

Figure 12: Velocity estimates in the kinematic mode. The first three panels show Northing, Easting and Up components of the velocity estimates and the bottom panel shows the residuals of the least-squares estimation for all satellites

As is illustrated in the last panel of Figure 11, compared with the residuals of the data recorded while the car was idling (that is, the data up to 225 seconds elapsed time), the residuals at the kinematic situations (that is, the data after 225 seconds elapsed time) were amplified and even biased. Figure 12 shows a few typical examples of the case in detail. Factors which can make such differences in the residuals may include the variation of receiver system noise, the higher-order effects of the receiver dynamics, and any other biases in the functional and stochastic models as defined in Eqs. (6) to (10).

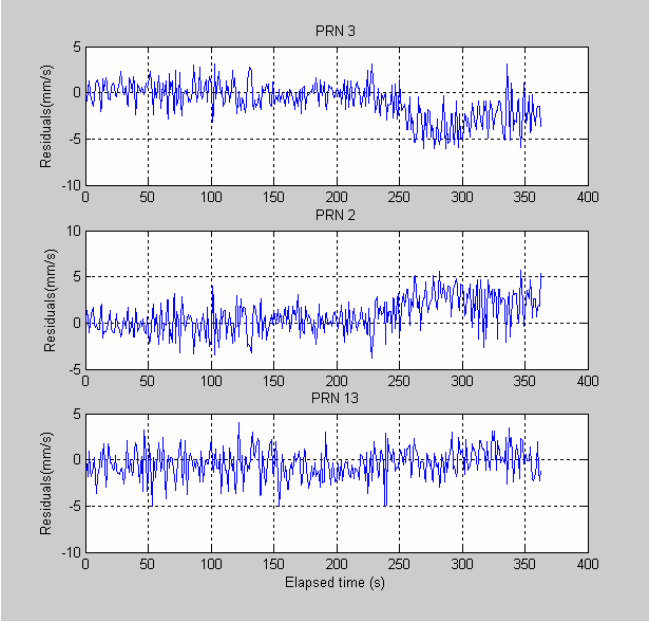

Figure 13: Residuals of the least-squares estimation for PRN 2, 3 and 13. The first two panels illustrate that the residuals are biased after 225 seconds elapsed time

In addition, we could mention that the phase measurement was degraded in the moving environment, since range error is a function of the noise bandwidth of the carrier tracking loop and signal-to-noise ratio (Spilker 1978). For the same noise bandwidth, lower signal-to-noise ratio degrades the range determination. Attenuation of the signal through its propagation path and increase of noise due to multipath are the principal cause of lowering signal-to-noise ratio. When the car was in movement after the 225 seconds elapsed time, we see an ondulation in the residuals of individual satellites in Figure 13. This fact could justify the belief that there is some evidence of multipath.

Since we use the first order central difference approximation of the carrier-phase rate for velocity determination, this approximation cannot reflect quite well the receiver dynamics in kinematic situations. The first order central difference approximation is a linear prediction of the Doppler shift which corresponds to a band-pass filter with cut-off frequencies at 0.125 and 0.375 Hz. The cut-off frequency of the filter is determined at the frequency where the amplitude reaches around 70% (i.e., $1/\sqrt{2}$) of the maximum amplitude. Figure 14 shows the frequency response of the filter to the amplitude at a 1 Hz sampling rate. The fourth-order Butterworth filter with cut-off frequencies at 0.125 and 0.375 Hz is also plotted in the figure as an example of the conventional band-pass filters which have more or less similar frequency responses.

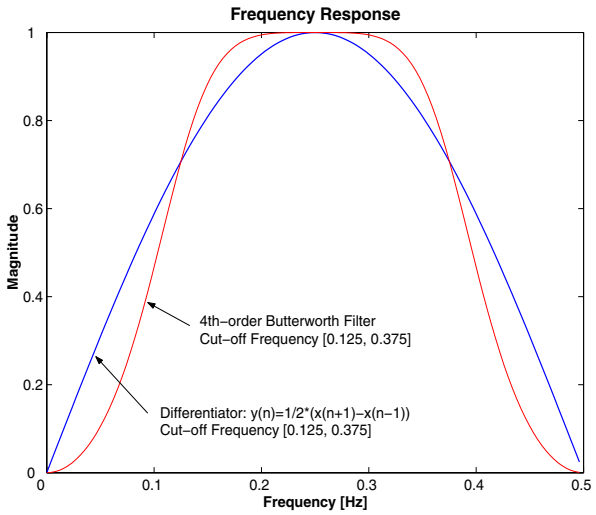

Figure 14: Frequency responses of the first order central difference approximation of the carrier-phase rate and the fourth-order Butterworth filter at a 1 Hz sampling rate

As is illustrated in Figure 14, the filter of the first order central difference approximation stops the signals at 0 and 0.5 Hz (i.e., Nyquist frequency). At a half of the Nyquist frequency (0.25 Hz), this filter passes the signals without filtering. Therefore, this filter can perfectly remove constant biases in the signals. However, this filter will reduce the amplitudes of the signals over all frequency components except for a half of the Nyquist frequency. As we carried out the kinematic test at a 1 Hz data rate, the higher-order effects (e.g., all frequency components higher than the Nyquist frequency, 0.5 Hz) of the receiver dynamics will be aliased in the approximation of the carrier phase [Ifeachor and Jervis, 1993]. These two facts (that is, signal reduction due to filtering and aliasing due to sampling) may explain why the velocity estimates and hence the residuals could be biased in the kinematic situations.

Another issue which may affect the residuals in kinematic situations is the stochastic model. We also used the exponential function of the elevation angle in Eqs. (8) to (10) for the kinematic test. As was described by Kim and Langley [2001], however, it should be noted that the elevation-angle dependence of the system noise often varies with the particular kinematic situation. The elevation-angle dependence of the system noise is induced mainly by the receiver antenna's gain pattern, with other factors such as atmospheric signal attenuation. The elevation angle is normally computed with respect to the local geodetic horizon plane at the antenna phase center regardless of the actual orientation of the antenna. Accordingly, the exact relationship between antenna gain and the signal elevation angle may be difficult to assert when the antenna orientation is changing which can happen often in kinematic situations such as going up or down hills or making banking turns.

CONCLUDING REMARKS

We have investigated the feasibility of a low-cost GPS velocity sensor for applications such as vehicle testing. We developed post-processing software which uses the first order central difference approximation of the carrier-phase rate. The advantage of this approximation is simplicity, which facilitates eventual implementation of algorithms into the receiver.

In this paper, we mainly focused on the scientific aspects of the GPS velocity determination. We investigated the potential accuracy which can be achieved with low-cost receivers, and evaluate the error budget present in the estimation.

We conducted field tests to verify the performance of our algorithm in static and kinematic mode. In static mode, the user velocity can be estimated to better than 1 cm/s (2-sigma) under high-multipath conditions. In kinematic mode, we observed the effect of the increase of receiver dynamics in the residuals. However, we did not experience any long signal interruption even under high-multipath.

Using the Doppler measurements (either the receiver-generated Doppler or the carrier-phase derived Doppler) observed from a moving platform, it is easy to determine the velocity of the platform as long as the satellite velocity is precisely known. We confirmed that the satellite velocity predicted by using the broadcast ephemeris in the navigation message is sufficient accurate by comparison to the velocity of SP3 precise ephemeris.

The errors in the position of a moving vehicle cause errors in the calculation of radial velocity. For stand-alone velocity determination, in order to achieve a solution at the mm/s level, satellite positions have to be known to better than 10 m.

Factors which can affect the velocity estimates may include the residuals of the satellite velocity prediction, the higher-order effects of receiver dynamics and errors such as residual atmospheric (ionospheric and tropospheric) delay, multipath and receiver system noise.

This paper gave a first look at the achievable accuracy of a low-cost velocity sensor. We will continue to investigate the potential accuracy which can be achieved with this kind of receiver, and evaluate the error budget present in the estimation, and then use this knowledge to develop more robust and reliable techniques which will be applied and tested, and embedded in a comprehensive navigation algorithm.

ACKNOWLEDGMENTS

This work described in this paper was supported by Furuno Electric Co., Ltd. and the Natural Sciences and Engineering Research Council of Canada.

We would like to thank C. S. Kang for helpful discussions.

REFERENCES

Bisnath, S. B. and R. B. Langley (2002). High Precision Kinematic Positioning with a Single GPS Receiver, Navigation; Journal of The Institute of Navigation, Vol. 49, No. 3, Fall 2002, pp. 161-169.

Collins, J.P. and R.B. Langley (1997). Estimating the Residual Tropospheric Delay for Airborne Differential GPS Positioning. Proceedings of the 10th International Technical Meeting of the Satellite Division of the Institute of Navigation, Kansas City, Missouri, 16-19 September, pp. 1197-1206.

Hatch, R. (1982). Synergism of GPS Code and Carrier Measurements, Proceedings of the 3rd International Geodetic Sypomsium on Satellite Doppler Positioning, Las Cruces, New Mexico, February, Vol. 2, pp. 1213-1232.

ICD-GPS-200C (1999). *Navstar GPS Space Segment/Navigation User Interface Control Document*, GPS Navstar JPO, 138 pp.

Ifeachor, E. C. and B. W. Jervis (1993*). Digital Signal Processing: A Practical Approach*. Addison-Wesley Publishing Co., Workingham, England.

Itani, K., T. Hayashi and M. Ueno (2000). Low-Cost Wave Sensor Using Time Differential Carrier Phase Observations, Proceedings of ION GPS 2000, Salt Lake City, Utah, 19-22 September 2000.

Jin, X. (1996). *Theory of Carrier Adjusted DGPS Positioning Approach and Some Experimental Results*, Delft University Press, Delft, The Netherlands, 162 pp.

Kaplan, E.D. (Ed.) (1996). *Understanding GPS, Principles and Applications*, Artech House Publishers, Boston-London, 554 pp.

Kim, D. and R.B. Langley (2001). Estimation of the Stochastic Model for Long-Baseline Kinematic GPS Applications, Proceedings of ION NTM 2001, Long Beach, California, 22-24 January 2001.

Misra, P. and P. Enge (2001), *Global Positioning System: Signals, Measurements, and Performance*, Ganga-Jamuna Press, Lincoln, Massachussets, 390 pp.

Niell, A.E. (1996). Global Mapping Functions for the Atmosphere Delay at Radio Wavelengths. Journal of Geophysical Research, Vol. 101, No. B2, pp. 3227-3246.

Okamura, K., Tokuyama, K. Sugimoto, S. Higuchi, T. and K. Takahata (2003). Development of Vehicle Trajectory Measurement System Using Stand-alone GPS, Presented at Vehicle Technology Conference, Yokohama, Japan, 4 pp. [in Japanese].

Ryan, S., G. Lachapelle and M. E. Cannon (1997). DGPS Kinematic Carrier Phase Signal Simulation Analysis in the Velocity Domain, Proceedings of ION GPS 97, Kansas City, Missouri, 16-19 September 1997.

Saastamoinen, J. (1973). Contributions to the Theory of Atmospheric Refraction. In three parts. Bulletin Géodésique, No. 105, pp. 279-298; No. 106, pp. 383-397; No. 107, pp. 13-34.

Spilker, J.J. (1978). GPS Signal Structure and Performance Characteristics, Navigation, Journal of the U.S. Institute of Navigation, Vol. 25, No. 2, Summer, pp. 121-146.

Szarmes, M., S. Ryan, G. Lachapelle and P. Fenton (1997). DGPS High Accuracy Velocity Determination Using Doppler Measurements, Proceedings of KIS 97, Department of Geomatics Engineering, The University of Calgary, Banff, 3-6 June 1997.

Ueno, M., K. Itani and T. Hayashi (2003). Développement d'un Capteur de Guidage Automatique Peu Coûteux pour des Véhicules Agricoles. Navigation-Paris, Journal of the French Institute of Navigation, Vol.51, No. 204, pp. 26-41 [in French].

Van Graas, F. and A. Soloviev (2003). Precise Velocity Estimation Using a Stand-Alone GPS Receiver, Proceedings of ION NTM 2003, Anaheim, California, 22-24 January 2003.